THE JOURNAL OF PHYSICAL CHEMISTRY C

Article

pubs.acs.org/JPCC

Electronic Relaxation in Benzaldehyde Evaluated via TD-DFT and Localized Diabatization: Intersystem Crossings, Conical Intersections, and Phosphorescence

Qi Ou and Joseph E. Subotnik*

Department of Chemistry, University of Pennsylvania, Philadelphia, Pennsylvania 19104, United States

ABSTRACT: The photophysics of benzaldehyde are analyzed through the lens of TD-DFT adiabatic excited states and Boys or Edmiston−Ruedenberg localized diabatic states. We predict rate constants for two processes in excited benzaldehyde: (i) the intersystem crossing from $S_1 \rightarrow T_2$ and (ii) the phosphorescence from $T_1 \rightarrow S_0$. We also study (iii) the conical intersection between T_2 and T_1 that is putatively responsible for an ultrafast internal conversion process, $T_2 \rightarrow T_1$. In agreement with Ohmori et al. (*J. Phys. Chem.* **1988**, *92* (5), 1086−1093), our results suggest that the $S_1 \rightarrow T_2$ intersystem crossing in benzaldehyde is rapid not only because of a large spin−orbit matrix element (i.e., El-Sayed's rule) but also because of a fortuitously small energy barrier. Furthermore, when studying the $T_2 \rightarrow T_1$ internal conversion, we find that both Boys and Edmiston−Ruedenberg localization give remarkably stable and accurate diabatic states which will be useful for ongoing studies of dynamics near conical intersections. To our knowledge, this is the first example whereby *localized* diabatization techniques have been tested and have successfully recovered the topology of a conical intersection.

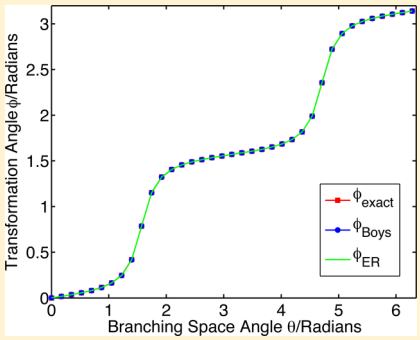

I. INTRODUCTION

A. Benzaldhye and Its Cascade of Electronic Relaxation. The photophysical processes of benzaldehyde have been extensively studied for decades.[1−10] It is commonly accepted that most aromatic carbonyl compounds, exemplified by benzaldehyde, benzophenone, etc., are weakly fluorescent, processing a very small value of fluorescence quantum yield ($\Phi_F \sim 0.0001-0.01$) when compared to that of aromatic hydrocarbons ($\Phi_F \sim 0.1-1$).[11] Assuming the electronic relaxation is not purely vibronic, this feature implies a relatively fast intersystem crossing (ISC) process for aromatic carbonyls from the singlet state to the triplet state, which is putatively promoted by strong spin−orbit couplings.[11] The robust phosphorescence of aromatic ketones also suggests a fast ISC process, which further highlights the importance of ISC in studies of the functional properties of organic chromophores. Because benzaldehyde is the smallest aromatic carbonyl compound, and because the molecule phosphoresces intensely, quantifying the transient photophysics of benzaldehyde is essential for a broad understanding of electronic relaxation in organic molecules with triplet channels.

As a practical matter, benzaldehyde is known to have a complex manifold of n−π^* and $\pi-\pi^*$ excited states, both singlet and triplet. Previous experimental results[1−6] show that the two lowest excited singlet states, S_1 and S_2, are assigned to n−π^* and $\pi-\pi^*$ transitions, respectively. While benzaldehyde dissociates to benzene and carbon monoxide after being excited to the S_2 state, according to both photolysis[2,12] and multiphoton ionization (MPI) experiments,[13−15] if we consider only photophysical processes (without bond making or breaking), then there are only four states of interest for benzaldehyde: S_0, S_1, T_1, and T_2. For convenience, see the schematic graph shown in Figure 1.

The origin of S_1(n−π^*) is found to lie 26 919 cm^{-1} above the ground state with weak intensity as measured by sensitized phosphorescence excitation spectrum.[1] Following excitation to the S_1 state, benzaldehyde undergoes a rapid ISC to the $\pi-\pi^*$ triplet state.[1,16−19] The efficiency of $S_1 \rightarrow T$ ISC is near unity in the vapor phase according to the absorption and phosphor-

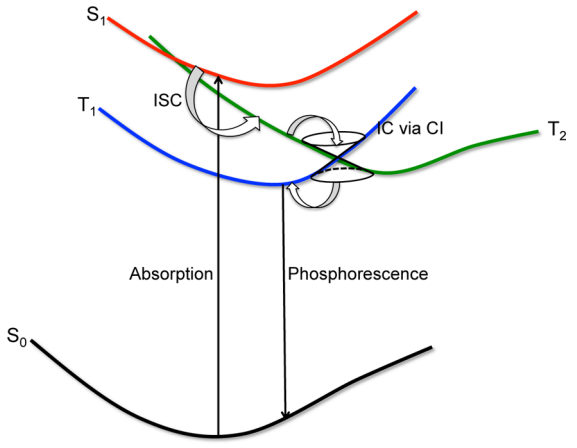

Figure 1. Schematic graph of the photophysical process in benzaldehyde.

Received: June 5, 2013
Revised: August 27, 2013
Published: August 29, 2013

   dx.doi.org/10.1021/jp405574q | *J. Phys. Chem. C* 2013, 117, 19839−19849

escence excitation spectra.[20] The two lowest triplet states, $T_1(n-\pi^*)$ and $T_2(\pi-\pi^*)$, are found lying below the S_1 state and close to each other, whereas only the $n-\pi^*$ triplet state has been successfully located in the gas phase.[1,2,7,21,22] The band origin of $T_1(n-\pi^*)$ lies ~25 180 cm^{-1} above the ground state from the phosphorescence excitation spectrum of isolated benzaldehyde,[1,22] which is slightly below the S_1 origin. Experimental data obtained from spectroscopic studies of beam-isolated benzaldehyde implicitly shows that the slight congestion of spectral lines in excess vibrational energy of 1 000−1 350 cm^{-1} above the $T_1(n-\pi^*)$ origin can be attributed to the onset of the $T_2(\pi-\pi^*)$ state.[22] The interconversion of these two states has also been observed in the same study, implying an efficient internal conversion (IC) from the $T_2(\pi-\pi^*)$ to the $T_1(n-\pi^*)$ state, the latter being the so-called phosphorescent state.[5]

B. Previous Computational Studies. Several theoretical studies have been carried out to explain the various photophysical processes in benzaldehyde.[3,8−10,16,18,23−25] Both ISC and IC contribute to the highly phosphorescent character of benzaldehyde by forcing the molecule into the T_1 state and therefore must be addressed. First, regarding ISC, several authors[1,9,23,26,27] have shown qualitatively the fast ISC between S_1 and $T_2(\pi-\pi^*)$ states following El-Sayed rules.[28] To our knowledge, however, quantitative estimates of the ISC rate constant have not been calculated using modern electronic structure theory.

Second, the IC between $T_1(n-\pi^*)$ and $T_2(\pi-\pi^*)$ has been identified recently by several groups with a conical intersection (CI) of interest.[9,10,24] Interestingly, W. Fang et al.[10,24] and G. Cui et al.[9] both predict that the T_1/T_2 CI point of lowest energy is nearly degenerate with S_1. While these authors have used highly accurate multiconfigurational levels of theory, CASSCF and CASPT2, the demanding cost of their calculations has precluded the study of the topology of the T_1/T_2 CI seam, and the rich dynamics of the corresponding internal conversion have not been fully investigated.

C. Outline and Motivation. In this work, we will quantitatively investigate the electronic relaxation processes in benzaldehyde via time-dependent density functional theory (TD-DFT) with a long-range corrected functional ωB97X,[29] working in the Tamm−Dancoff approximation. Because ωB97X includes exact Hartree−Fock exchange in both short and long-range, it is believed to be an effective way of dealing with charge-transfer states.[29] Taking advantage of the cheap computational cost of TD-DFT, our central goal is to explore the dynamics and photophysics of benzaldehyde, quantitatively studying both radiationless processes (i.e., (i) ISC and (ii) IC) as well as (iii) the phosphorescence from the T_1 state to the ground state. An outline of this paper is as follows: The optimized geometries and excitation energies are evaluated in Section II, followed by the analysis of the S_1/T_2 spin−orbit coupling and ISC in Section III. In Section IV, we investigate the T_1/T_2 CI at which point we will assess the validity of localized diabatization methods. Finally, in Section V, the phosphorescence lifetime of benzaldehyde from T_1 to the ground state will be evaluated.

There is always some ambiguity for the notation of the electronic states for any system displaying an electronic crossing or CI. For convenience, we will use T_1 and T_2 to denote the diabatic states $T(n-\pi^*)$ and $T(\pi-\pi^*)$, respectively, as shown in Figure 1. The energy of T_2 may be less than that of T_1 at certain geometries because of the mixing between them, but hopefully our notation will always be clear.

II. EVALUATION OF THE OPTIMIZED GEOMETRIES AND EXCITATION ENERGIES

A. Optimized Structures for S_0, S_1, and T_1. Every study of electronic relaxation begins with potential energy surfaces. The geometries of the four states of interest for benzaldehyde (S_0, S_1, T_1, and T_2) were each optimized with the ωB97X functional using a 6-31G** basis. The ab initio quantum chemistry package Q-Chem was employed for all calculations.[30] The character of each excited-state transition was analyzed by the attachment−detachment[31] densities shown in Figure 2, indicating that S_1, T_1, and T_2 involve $n-\pi^*$, $n-\pi^*$, and $\pi-\pi^*$ transitions, respectively.

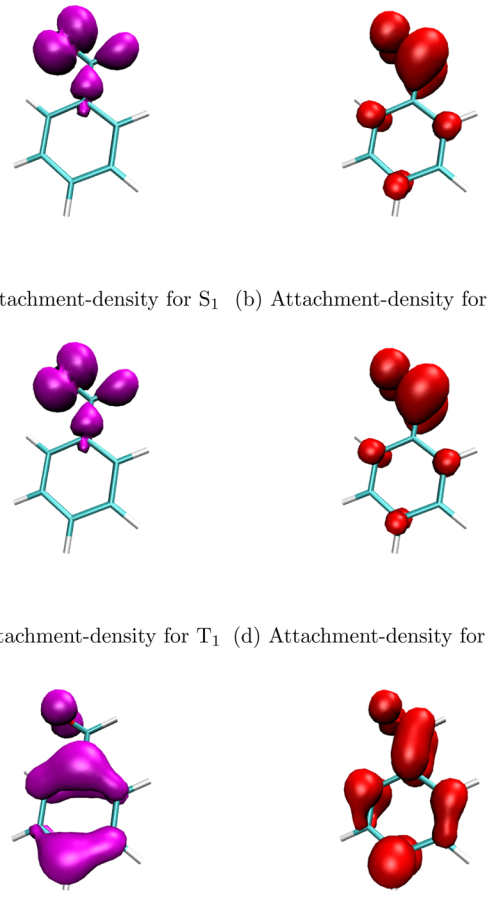

(a) Detachment-density for S_1 (b) Attachment-density for S_1 ($n-\pi^*$)

(c) Detachment-density for T_1 (d) Attachment-density for T_1 ($n-\pi^*$)

(e) Detachment-density for T_2 (f) Attachment-density for T_2 ($\pi-\pi^*$)

Figure 2. Attachment−detachment[31] densities for S_1, T_1, and T_2 states at their optimized geometries.

Parameters for the four optimized structures are shown in Table 1 with the corresponding atoms shown in Figure 3. All of the optimized geometries have a nearly planar shape. The S_0 optimized geometry shows a typical phenyl ring with an average 1.392 Å C−C bond length, and the C═O bond length here is 1.210 Å. The structures at S_1 and T_1 optimized geometries are quite similar, perhaps because they both carry a $n-\pi^*$ transition. Compared with the ground state, the most prominent change in geometry for the two $n-\pi^*$ states is

dx.doi.org/10.1021/jp405574q | J. Phys. Chem. C 2013, 117, 19839−19849

Table 1. Experimental and Computational Results for the Key Geometric Parameters (in Å for Bond Length and Degree for Angles) of Benzaldehyde in Different Optimized Geometries

parameter	S_0-loc-min[a]	S_1-loc-min	T_1-loc-min	T_2-loc-min[a]
C1−C2	1.396 (1.388 ± 0.004)	1.410	1.408	1.478 (1.479 ± 0.029)
C2−C3	1.387 (1.381 ± 0.004)	1.388	1.389	1.360 (1.322 ± 0.029)
C3−C4	1.395	1.392	1.391	1.422
C4−C5	1.392	1.397	1.396	1.450
C5−C6	1.390 (1.381 ± 0.004)	1.382	1.384	1.352 (1.322 ± 0.029)
C1−C6	1.394 (1.388 ± 0.004)	1.412	1.409	1.460 (1.479 ± 0.029)
C1−C7	1.483 (1.480 ± 0.005)	1.431	1.437	1.414 (1.420 ± 0.045)
C7−O	1.210 (1.200 ± 0.002)	1.293	1.297	1.255 (1.263 ± 0.031)
C1−C7−O	124.2 (126.4 ± 0.3)	124.3	123.3	122.2 (125.4 ± 2.6)
C2−C1−C7	119.7	121.1	121.6	119.4

[a]Values in parentheses are experimental data given by Zewail and co-workers via the UED method, with 3σ error bars. C_{2v} symmetry was imposed for the phenyl ring in the experimentally fit results. See ref 16.

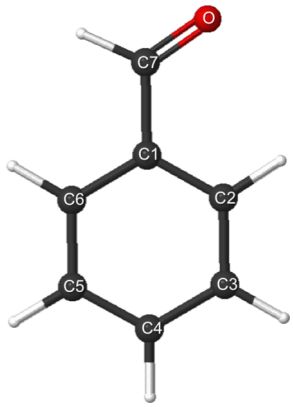

Figure 3. Schematic structure of benzaldehyde.

that the C═O bond is elongated to around 1.295 Å and the distance between the carbonyl group and the phenyl ring is shortened by about 0.05 Å. This geometric difference is caused by the fact that the n−π^* transition couples strongly to the C═O stretching mode, which greatly changes the position of C7 and O while marginally influencing the phenyl ring. The optimized geometry of the T_2 state, which has the π−π^* character, shows a standard quinoid-type structure, and the average C−C bond length of the aromatic ring is increased by 0.03 Å. These optimized parameters are consistent with the experimental data given by Zewail and co-workers via ultrafast electron diffraction (UED),[16] which to some extent shows the reliability of the TD-DFT/ωB97X approach to dealing with the benzaldehyde system.

B. Adiabatic and Vertical Excitation Energies. The adiabatic energies of S_1, T_1, and T_2 states are shown in Table 2. The adiabatic energy of the S_1 excited states is the energy of S_1 at the optimized geometry for S_1 minus the energy of S_0 at the optimized ground state geometry; the adiabatic energy of T_1 and T_2 are calculated in a similar fashion. Compared with experimental values,[1] the results given by TD-DFT/ωB97X are consistent for the triplet states and are much more satisfying than those given by configuration interaction singles (CIS), which orders the triplet states incorrectly. As might be expected, CIS overestimates the excitation energy of the n−π^* states because of the charge-transfer character.[32] The excitation energy of the S_1 state is overestimated by ∼0.4 eV. A complete set of S_0, S_1, T_1, and T_2 energies at all possible optimized geometries is shown in Table 3, along with a comparison of the CASPT2 results given by V. Molina et al.[8] The good agreement between these two methods confirms the validity of the TD-DFT/ωB97X for both charge-transfer states and noncharge-transfer states in benzaldehyde.

Table 2. Experimental and Theoretical Results for the Adiabatic Excitation Energies (in eV) of S_1, T_1, and T_2 States

state	CIS	TD-DFT/ωB97X	experimental data[a]
T_1	3.94	3.17	3.12
T_2	2.85	3.34	3.30
S_1	4.64	3.75	3.34

[a]Given by Ohmori et al.[1]

Table 3. Comparison of S_0, S_1, T_1, and T_2 Relative Energies (in eV) at Different Optimized Geometries for TD-DFT/ωB97X (versus CASPT2 Reference Energies)

state	S_0-loc-min	S_1-loc-min	T_1-loc-min	T_2-loc-min
S_0	0(0)	0.30(0.57)	0.33(0.48)	0.49(0.37)
S_1	4.01(3.71)	3.75(3.27)	3.76(3.29)	4.07(3.76)
T_1	3.45(3.40)	3.18(3.07)	3.17(3.07)	3.53(3.52)
T_2	3.78(3.49)	3.64(3.39)	3.64(3.40)	3.34(3.16)

III. S_1/T_2 SPIN−ORBIT COUPLING AND INTERSYSTEM CROSSING RATE

It is well-known that benzaldehyde's highly phosphorescent character is caused by a very fast ISC process between the n−π^* singlet state and the π−π^* triplet state. To analyze the rate of ISC, the one-electron Breit−Pauli Hamiltonian[33] was employed to calculate the S_1/T_2 spin−orbit coupling

$$\hat{H}_{SO} = -\frac{\alpha_0^2}{2}\sum_{i,A}\frac{Z_A}{r_{iA}^3}(\mathbf{r}_{iA}\times\mathbf{p}_i)\cdot\mathbf{s}_i \quad (1)$$

where i denotes electrons and A denotes nuclei. $\alpha_0 = 137.037^{-1}$ is the fine structure constant. Z_A is the bare positive charge on nucleus A. In the second quantization representation, the spin−orbit Hamiltonian in different directions can be expressed as

$$\hat{H}_{SO_x} = -\frac{\alpha_0^2}{2}\sum_{pq}\tilde{L}_{xpq}\frac{\hbar}{2}(a_p^\dagger a_{\bar{q}} + a_{\bar{p}}^\dagger a_q) \quad (2)$$

dx.doi.org/10.1021/jp405574q | J. Phys. Chem. C 2013, 117, 19839−19849

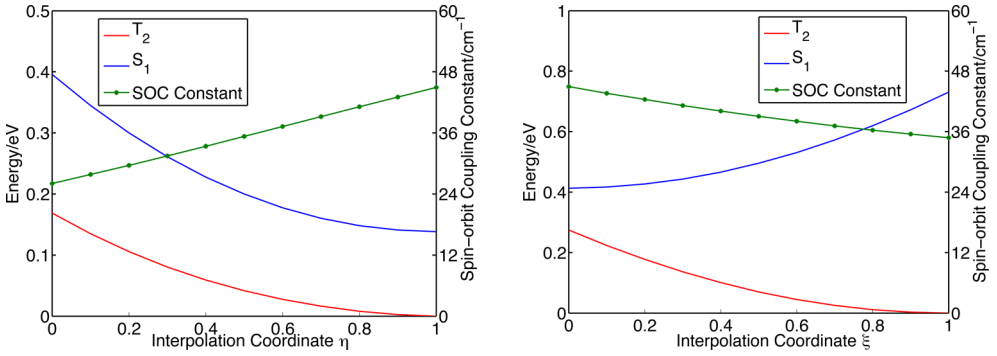

Figure 4. S_1/T_2 spin−orbit coupling constant along two different interpolation coordinates, η and ξ. On the left, $\eta = 0$ refers to the Franck−Condon point of the S_1 state, and $\eta = 1$ refers to S_1 local minimum. On the right, $\xi = 0$ refers to S_1 local minimum, and $\xi = 1$ refers to T_2 local minimum.

$$\hat{H}_{SO_y} = -\frac{\alpha_0^2}{2}\sum_{pq}\tilde{L}_{ypq}\frac{i\hbar}{2}(a_p^\dagger a_{\bar{q}} - a_{\bar{p}}^\dagger a_q) \tag{3}$$

$$\hat{H}_{SO_z} = -\frac{\alpha_0^2}{2}\sum_{pq}\tilde{L}_{zpq}\frac{\hbar}{2}(a_p^\dagger a_q - a_{\bar{p}}^\dagger a_{\bar{q}}) \tag{4}$$

where $\tilde{L}_\alpha = L_\alpha/r^3$ $(\alpha = x, y, z)$. The single-reference ab initio excited states (within the Tamm−Dancoff approximation) are given by

$$|\Phi_{\text{singlet}}\rangle = \sum_{i,a} s_i^a(a_a^\dagger a_i + a_{\bar{a}}^\dagger a_{\bar{i}})|\Phi_{\text{HF}}\rangle \tag{5}$$

$$|\Phi_{\text{triplet}}^{m_s=0}\rangle = \sum_{i,a} t_i^a(a_a^\dagger a_i - a_{\bar{a}}^\dagger a_{\bar{i}})|\Phi_{\text{HF}}\rangle \tag{6}$$

$$|\Phi_{\text{triplet}}^{m_s=1}\rangle = \sum_{i,a} \sqrt{2}\, t_i^a a_a^\dagger a_{\bar{i}}|\Phi_{\text{HF}}\rangle \tag{7}$$

$$|\Phi_{\text{triplet}}^{m_s=-1}\rangle = \sum_{i,a} \sqrt{2}\, t_i^a a_{\bar{a}}^\dagger a_i|\Phi_{\text{HF}}\rangle \tag{8}$$

where s_i^a and t_i^{a34} are singlet and triplet excitation coefficients, respectively, with the normalization $\Sigma_{ia}s_i^{a2} = \Sigma_{ia}t_i^{a2} = {}^1/_2$; $|\Phi_{\text{HF}}\rangle$ refers to the Hartree−Fock ground state. Thus, the spin−orbit coupling constant from the singlet state to different triplet manifolds can be obtained as follows:

$$\langle\Phi_{\text{singlet}}|\hat{H}_{\text{SO}}|\Phi_{\text{triplet}}^{m_s=0}\rangle = \frac{\alpha_0^2\hbar}{2}\left(\sum_{i,a,b}\tilde{L}_{zab}s_i^a t_i^b - \sum_{i,j,a}\tilde{L}_{zij}s_i^a t_j^a\right) \tag{9}$$

$$\langle\Phi_{\text{singlet}}|\hat{H}_{\text{SO}}|\Phi_{\text{triplet}}^{m_s=\pm1}\rangle = \mp\frac{\alpha_0^2\hbar}{2\sqrt{2}}\left(\sum_{i,a,b}\tilde{L}_{xab}s_i^a t_i^b - \sum_{i,j,a}\tilde{L}_{xij}s_i^a t_j^a\right) + \frac{\alpha_0^2\hbar}{2\sqrt{2}}\left(\sum_{i,a,b}\tilde{L}_{yab}s_i^a t_i^b - \sum_{i,j,a}\tilde{L}_{yij}s_i^a t_j^a\right) \tag{10}$$

The total (root mean square) spin−orbit coupling is given by

$$\langle\Phi_{\text{singlet}}|\hat{H}_{\text{SO}}|\Phi_{\text{triplet}}\rangle = \sqrt{\sum_{m_s=0,\pm1}\left\|\langle\Phi_{\text{singlet}}|\hat{H}_{\text{SO}}|\Phi_{\text{triplet}}^{m_s}\rangle\right\|^2} \tag{11}$$

Figure 4 shows the total spin−orbit coupling constant for S_1/T_2 as a function of nuclear geometry. The two interpolation coordinates are defined as

$$R(\eta) = R_{S_0} + \eta(R_{S_1} - R_{S_0}) \tag{12}$$

$$R(\xi) = R_{T_2} + \xi(R_{T_2} - R_{S_1}) \tag{13}$$

where R_{S_0}, R_{S_1}, and R_{T_2} (in Cartesian coordinates) refer to the local minima of S_0, S_1, and T_2 states, respectively.

The coupling is found to be stronger during the relaxation process of the S_1 state, increasing from ∼26 cm^{-1} to ∼45 cm^{-1}, which is quite large for organic compounds, and it slightly decreases to ∼35 cm^{-1} from the S_1 local minimum to the T_2 local minimum. Following El-Sayed rules, we mention that the coupling between S_1 and T_1 is less than 0.3 cm^{-1} because the n−π^* state couples weakly to another n−π^* state.

Because the spin−orbit coupling is relatively weak and the coupling element does not significantly depend on nuclear geometry, Marcus theory[35] can be applied to calculate the ISC rate constant from S_1 to the T_2 manifold[36,37]

$$k_{\text{ISC}} = \frac{2\pi}{\hbar}\|\langle H_{\text{SO}}\rangle_{if}\|^2\sqrt{\frac{1}{4\pi k_B T}}\exp\left(-\frac{(\lambda + \Delta G)^2}{4\lambda k_B T}\right) \tag{14}$$

where $\|\langle H_{\text{SO}}\rangle_{if}\|$ is the spin−orbit coupling constant between the initial state S_1 and the final T_2 state manifold (eq 11), λ the reorganization energy, and ΔG the driving force. As shown in Figure 5, λ is the energy of T_2 at the S_1 optimized geometry minus the minimum energy of T_2, which is 0.274 eV. ΔG is the energy difference between the T_2 minimum energy and the S_1

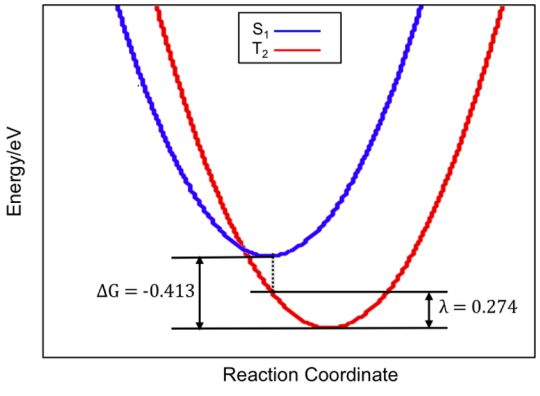

Figure 5. Graphical representation of the reorganization energy λ and the activation energy ΔG in eV.

dx.doi.org/10.1021/jp405574q | J. Phys. Chem. C 2013, 117, 19839−19849

minimum energy, which is −0.413 eV. Evaluating H_{SO} at the S_1 optimized geometry, the S_1/T_2 ISC rate constant k_{ISC} given by eq 14 is 8.03×10^{10} s^{-1} ($1/k_{ISC}$ = 12.5 ps), which is the same order as the ISC rate constant of other carbonyl compounds possessing close-lying $S_1(n-\pi^*)$ and $T(\pi-\pi^*)$ states such as benzophenone;[11] needless to say, this rate is much faster than the normal ISC time scale ($\sim 10^{-8}-10^{-3}$ s).[38] Our result is also close to the ISC rate constant for benzaldehyde given by S. T. Park et al.[17] via the UED experiment, which was 2.4×10^{10} s^{-1}. Occurring in the picosecond domain, this remarkably fast ISC process between the S_1 and T_2 states, and subsequently followed by the efficient T_1/T_2 IC via the CI, which is expected to be on the order of the vibrational period,[10] explains both the short lifetime of the S_1 state and the fact that benzaldehyde is highly phosphorescent but only weakly fluorescent (without considering the radiationless decay from S_1).

IV. CONICAL INTERSECTIONS AND LOCALIZED DIABATIZATION METHODS

Mathematically, a point of CI is a geometry where different adiabatic electronic states are energetically degenerate.[39] The efficiency of the radiationless transition between two states depends critically on the derivative coupling between these two states,[40−42] which is inversely proportional to the energy difference. At a CI, where the energy difference vanishes, the derivative coupling goes to infinity, leading to the most efficient radiationless transitions possible. Recent computational advances have enabled the location of CIs, which turn out to be ubiquitous in polyatomic molecules[42] and play a key role in many nonadiabatic events.[39,43−47] Efficient algorithms have been proposed to locate the minimum energy point at a CI seam, most famously by Yarkony.[48] In this paper, we followed the straightforward approach from Martinez et al.,[49] whereby one applies a penalty function to minimize the energy difference between the adiabatic states and then minimizes the average state energy, perpetually increasing the penalty function.

A. Simple Model Hamiltonian and Exact Mixing Angle Starting from Diabats. To analyze a CI, the most standard route is to start with a simple model of a linear Hamiltonian in an exactly diabatic basis, $|\Xi_1\rangle$ and $|\Xi_2\rangle$, from which an adiabatic basis, $|\Psi_1(\mathbf{R})\rangle$ and $|\Psi_2(\mathbf{R})\rangle$, can be generated as follows

$$|\Psi_1(\mathbf{R})\rangle = |\Xi_1\rangle \cos\phi(\mathbf{R}) - |\Xi_2\rangle \sin\phi(\mathbf{R}) \tag{15}$$

$$|\Psi_2(\mathbf{R})\rangle = |\Xi_1\rangle \sin\phi(\mathbf{R}) + |\Xi_2\rangle \cos\phi(\mathbf{R}) \tag{16}$$

where $\mathbf{R}$ refers to the nuclear coordinates and ϕ is the mixing angle between adiabatic and diabatic states. The Hamiltonian in the diabatic basis can always be represented exactly as

$$\mathbf{H}(\mathbf{R}) = \begin{pmatrix} H_{11}(\mathbf{R}) & H_{12}(\mathbf{R}) \\ H_{21}(\mathbf{R}) & H_{22}(\mathbf{R}) \end{pmatrix} \equiv S(\mathbf{R})\mathbf{I} + \begin{pmatrix} -G(\mathbf{R}) & V(\mathbf{R}) \\ V(\mathbf{R}) & G(\mathbf{R}) \end{pmatrix} \tag{17}$$

where $S(\mathbf{R}) = [H_{11}(\mathbf{R}) + H_{22}(\mathbf{R})]/2$, $G(\mathbf{R}) = [H_{22}(\mathbf{R}) - H_{11}(\mathbf{R})]/2$, and $V(\mathbf{R}) = H_{12}(\mathbf{R})$. The mixing angle ϕ can be expressed in terms of the matrix elements of the Hamiltonian

$$\tan 2\phi = \frac{V(\mathbf{R})}{G(\mathbf{R})} \tag{18}$$

At a CI, two gradients of particular interest are defined as

$$\mathbf{g}(\mathbf{R}_{CI}) \equiv \nabla G(\mathbf{R}_{CI}) \tag{19}$$

$$\mathbf{h}(\mathbf{R}_{CI}) \equiv \nabla V(\mathbf{R}_{CI}) \tag{20}$$

where $\mathbf{R}_{CI}$ refers to the nuclear coordinates at the CI. $\mathbf{g}$ and $\mathbf{h}$ form the so-called *branching plane* or the $\mathbf{g}-\mathbf{h}$ *plane*,[39] in which the energy degeneracy is lifted linearly.

Through a first order approximation, the Hamiltonian at the branching plane can then be expressed as

$$\mathbf{H} = (s_1 x + s_2 y)\mathbf{I} + \begin{pmatrix} -gx & hy \\ hy & gx \end{pmatrix} \tag{21}$$

$$s_1 = \nabla(H_{11} + H_{22})\cdot\mathbf{x} \tag{22}$$

$$s_2 = \nabla(H_{11} + H_{22})\cdot\mathbf{y} \tag{23}$$

where $g = \|\mathbf{g}\|$, $h = \|\mathbf{h}\|$, and $\mathbf{x}$ and $\mathbf{y}$ are two perpendicular unit vectors which point in the directions of $\mathbf{g}$ and $\mathbf{h}$, respectively.[45]

B. Computing the Branching Plane and Exact Mixing Angle in Practice Starting from Adiabats. In practice, given that we can compute only adiabatic energies using electronic structure calculations, one can find the branching plane of a molecule as follows:

i. Find a CI point, $\vec{R}_{CI}$.

ii. Displace each of the 3N Cartesian coordinates in positive and negative directions, and at every displaced point perform (6N) gradient calculations for the adiabatic energies:

$$\vec{D}_i^{\pm} = \frac{1}{2}[\nabla E_2^{ad}(\vec{R}_{CI} \pm \Delta R\cdot\vec{e}_i) - \nabla E_1^{ad}(\vec{R}_{CI} \pm \Delta R\cdot\vec{e}_i)],\ i = 1, ..., 3N \tag{24}$$

iii. Notice that all 3N gradients actually lie in a single 2D plane, the $\mathbf{g}-\mathbf{h}$ branching plane. At this point, we must make a nonunique choice of $\mathbf{g}$ and $\mathbf{h}$ that corresponds to a unique diabatic basis.

iv. In our calculations, we check the energy difference gradient $\vec{D}$ along a circle that is centered at $\vec{R}_{CI}$ in the $\mathbf{g}-\mathbf{h}$ plane. If θ is the angle of rotation around $\vec{R}_{CI}$, we have already computed $\vec{D}(\theta)$ in step ii. We define $\mathbf{g}$ as $\vec{D}(\theta_{max})$ when θ_{max} is chosen as the angle that maximizes $\|\vec{D}(\theta)\|$.

v. Finally, we check for the angle that minimizes $\|\vec{D}(\theta)\|$. By construction, $\vec{D}(\theta_{min})$ must be perpendicular to $\mathbf{g}$ and can be defined as $\mathbf{h}$. Note that these definitions fix a unique choice of diabatic states. If one were so inclined, one could construct $\mathbf{g}$ and $\mathbf{h}$ as nonorthogonal to each other using a different set of diabatic states, so long as one recovers the correct adiabatic energies around $\vec{R}_{CI}$:

$$E_{\pm} = s_1 x + s_2 y \pm \sqrt{g^2 x^2 + h^2 y^2} \tag{25}$$

Once the $\mathbf{g}$ and $\mathbf{h}$ vectors (and corresponding $x-y$ coordinates) are determined, the mixing angle between adiabatic and diabatic states can then be expressed in polar coordinates as

$$\sin 2\phi = \frac{h \sin\theta}{\sqrt{(g\cos\theta)^2 + (h\sin\theta)^2}} \tag{26}$$

$$\cos 2\phi = \frac{g \cos\theta}{\sqrt{(g\cos\theta)^2 + (h\sin\theta)^2}} \tag{27}$$

dx.doi.org/10.1021/jp405574q | J. Phys. Chem. C 2013, 117, 19839−19849

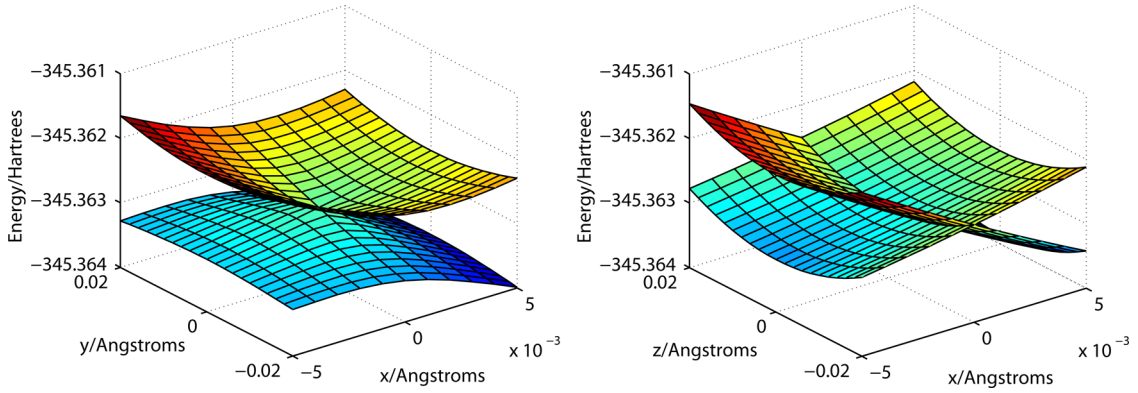

Figure 6. T_1/T_2 conical intersection of benzaldehyde. On the left, we plot the two potential energy surfaces in the branching plane. On the right, we plot the potential energy surfaces as the function of one coordinate, *x*, in the branching space and another random coordinate in the seam space.

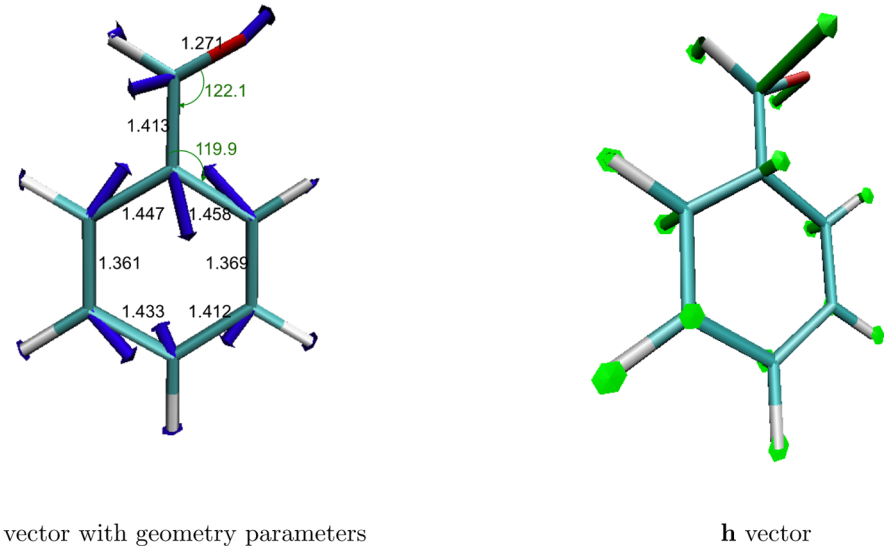

g vector with geometry parameters **h** vector

Figure 7. Energy-optimized structure of benzaldehyde along the CI seam (in Å for bond length and degrees for angles) and **g** and **h** vectors. The **g** vector is roughly in the plane, and the **h** vector is out of the plane.

where ρ and θ are defined by $x = \rho\cos\theta$ and $y = \rho\sin\theta$. For each different direction on the branching plane, ϕ can be solved in terms of *g*, *h*, and θ. ϕ does not depend on the radius ρ, i.e., the distance moving away from the CI point.

Before ending, we must address the subtlety that for a given subspace of adiabatic states there is, in general, no corresponding set of true diabats. As shown by Baer[50] and Mead and Truhlar,[51] rigorous diabats exist only if the curl condition is satisfied. Notwithstanding this limitation, approximately diabatic states can be constructed with small derivative couplings (e.g., ref 52), and there many formulations available in the literature to construct such quasi-diabatic states, e.g., configurational uniformity,[53,54] the fourfold way,[55−58] block-diagonalization,[59] generalized Mulliken−Hush (GMH),[60−62] Boys localization,[63] ER localization,[64] fragment charge difference (FCD),[65] fragment energy difference (FED),[66−68] and constrained DFT.[69−72] As such, we interpret eqs 26 and 27 as defining the *exact* mixing angle between adiabats and diabats.

C. The T_1/T_2 Conical Intersection in Benzaldehyde. With regard to the T_1/T_2 CI in benzaldehyde, we found an energetically low-lying CI (Figure 6). According to ωB97X, we did not find a low-lying three-state intersection as reported by Fang[10] and Cui.[9] If the CASSCF/CASPT2 calculations are reliable, then TD-DFT is overestimating the S_1 excitation energy relative to the triplet manifold.

The geometry of benzaldehyde at the CI is shown in Figure 7 along with the **g** and **h** vectors. The CI structure is quinoid-type with an elongated C═O bond, which are the characteristics of $T(\pi-\pi^*)$ and $T(n-\pi^*)$ states respectively. The **g** vector is along the molecular plane and contains the C−C stretching mode at the phenyl ring as well as the C═O stretching mode. The **h** vector, on the other hand, is perpendicular to the molecular plane and roughly follows the bending mode of the carbonyl group.

D. Localized Diabatization Method. The procedure used in Section IV.B for calculating diabatic states (and the branching plane) was tedious. Diabatic states are crucial for modeling the dynamics of the electron-transfer process and it is of great importance for calculating stable diabatic states from adiabatic states (as evidenced by the list of diabatization schemes referenced above). Given our focus on dynamics and our need for very fast diabatization algorithms, we have now applied localized diabatization methods to benzaldehyde.

The basic premise behind localized diabatization is to generate an adiabatic-to-diabatic rotation matrix by maximizing a localization function. Two well-known localization algorithms are Boys localization,[63] which maximizes the distance between

dx.doi.org/10.1021/jp405574q | J. Phys. Chem. C 2013, 117, 19839−19849

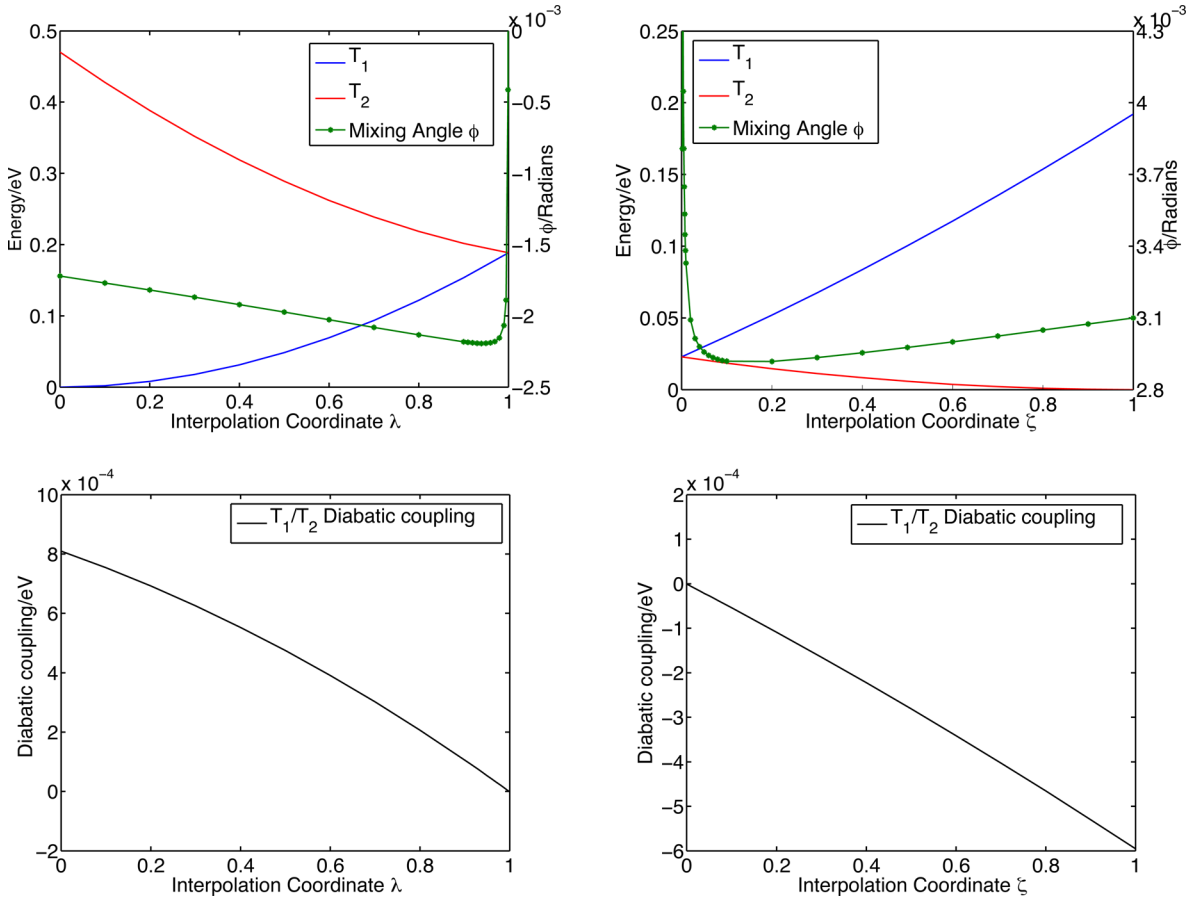

Figure 8. Potential energy surfaces, mixing angle (top panels), and diabatic coupling (bottom panels) along different paths. Both the mixing angle and the diabatic coupling are calculated by the Boys localized diabatization method. The left two plots are along the interpolation coordinate λ, where $\lambda = 0$ corresponds to the T_1 local minimum and $\lambda = 1$ corresponds to the CI point. The right two plots are along the interpolation coordinate ζ, where $\zeta = 0$ corresponds to the CI point and $\zeta = 1$ corresponds to the T_2 local minimum. Note that the mixing angle is plotted according to the (10^{-3}) radian scale on the right-hand axis and changes very little.

the centroids of different states, and Edmiston–Ruedenberg (ER) localization,[64] which maximizes the self-repulsion energy of the states. Boys and ER localized diabatization algorithms are analogous to Boys[73] and ER[74] orbital localization in quantum chemistry. In the realm of nonadiabatic dynamics, the Boys algorithm is a multistate generalization of Cave and Newton's generalized Mulliken–Hush algorithm (GMH).[60,61] The Boys and ER algorithms also have elements in common with Voityuk's FCD scheme[65] and Hsu's FED approach,[66−68] though the Boys and ER algorithms (unlike the FCD and FED approaches) do not require fragment definitions. All of these techniques fall under the title of localized diabatization.

Taking the two-state system as an example, diabatic states can be obtained via localized diabatization as follows:

i. Starting from two adiabatic states, $|\Psi_1\rangle$ and $|\Psi_2\rangle$, the localized diabatic states, $|\Xi_1^{\mathrm{LD}}\rangle$ and $|\Xi_2^{\mathrm{LD}}\rangle$, are constructed as a function of a rotation matrix $\mathbf{U}$

$$\begin{pmatrix} |\Xi_1^{\mathrm{LD}}\rangle \\ |\Xi_2^{\mathrm{LD}}\rangle \end{pmatrix} = \mathbf{U} \begin{pmatrix} |\Psi_1\rangle \\ |\Psi_2\rangle \end{pmatrix} \tag{28}$$

ii. The rotation matrix $\mathbf{U}$ is determined by maximizing the Boys or ER localization functions

$$f_{\mathrm{Boys}}(\mathbf{U}) = f_{\mathrm{Boys}}(|\Xi_1^{\mathrm{LD}}\rangle, |\Xi_2^{\mathrm{LD}}\rangle) = \sum_{i,j=1}^{2} |\langle \Xi_i^{\mathrm{LD}}|\vec{\mu}|\Xi_i^{\mathrm{LD}}\rangle - \langle \Xi_j^{\mathrm{LD}}|\vec{\mu}|\Xi_j^{\mathrm{LD}}\rangle|^2 \tag{29}$$

$$f_{\mathrm{ER}}(\mathbf{U}) = f_{\mathrm{ER}}(|\Xi_1^{\mathrm{LD}}\rangle, |\Xi_2^{\mathrm{LD}}\rangle) = \sum_{i=1}^{2} \int \mathrm{d}\mathbf{r_1} \int \mathrm{d}\mathbf{r_2} \frac{\langle \Xi_i^{\mathrm{LD}}|\hat{\rho}(\mathbf{r_1})|\Xi_i^{\mathrm{LD}}\rangle\langle \Xi_i^{\mathrm{LD}}|\hat{\rho}(\mathbf{r_2})|\Xi_i^{\mathrm{LD}}\rangle}{|\mathbf{r_1} - \mathbf{r_2}|} \tag{30}$$

Here, $\hat{\rho}(\mathbf{r})$ is the electronic density at position $\mathbf{r}$, i.e. $\hat{\rho}(\mathbf{r}) = \Sigma_i \delta(\hat{r}_i - \mathbf{r})$.

iii. Once the rotation matrix $\mathbf{U}$ is determined, the mixing angle ϕ_{Boys} or ϕ_{ER} can be obtained by

$$\mathbf{U}_{\mathrm{Boys}} = \begin{pmatrix} \cos\phi_{Boys} & \sin\phi_{\mathrm{Boys}} \\ -\sin\phi_{\mathrm{Boys}} & \cos\phi_{\mathrm{Boys}} \end{pmatrix} \tag{31}$$

$$\mathbf{U}_{\mathrm{ER}} = \begin{pmatrix} \cos\phi_{\mathrm{ER}} & \sin\phi_{\mathrm{ER}} \\ -\sin\phi_{\mathrm{ER}} & \cos\phi_{\mathrm{ER}} \end{pmatrix} \tag{32}$$

dx.doi.org/10.1021/jp405574q | J. Phys. Chem. C 2013, 117, 19839−19849

To our knowledge, the accuracy of localized diabatization methods has never been checked in the vicinity of a CI.[75]

In this work, we first verified the reliability of Boys localized diabatization by calculating the diabatic coupling along different interpolation coordinates. In Figure 8, the localized diabatization method is applied to the lowest two triplet states of benzaldehyde. The two paths are defined as

$$R(\lambda) = R_{T_1} + \lambda(R_{CI} - R_{T_1}) \quad (33)$$

$$R(\zeta) = R_{CI} + \zeta(R_{T_2} - R_{CI}) \quad (34)$$

where R_{T_1}, R_{T_2}, and R_{CI} (in Cartesian coordinates) refer to the local minima of the T_1 and T_2 states and the CI point respectively. The mixing angle is basically a constant along the two paths except at the CI point; note the scale on the right-hand axis in Figure 8. At the CI point itself, the adiabats (and thus ϕ) are undefined. The diabatic coupling near the CI point is almost zero, and changes nearly linearly along the two interpolation coordinates. This is qualitatively consistent with the topology of a CI (see eqs 21 and 26).

Second, as an even stronger means of validating these techniques of a localized dibatization, we compare ϕ_{Boys}/ϕ_{ER} with the absolute mixing angle ϕ_{exact}, which can be calculated around the CI (see eqs 26 and 27). As shown in Figure 9, the perfect agreement between the mixing angles truly proves the reliability of both the Boys and ER localized diabatization methods around the CI area.

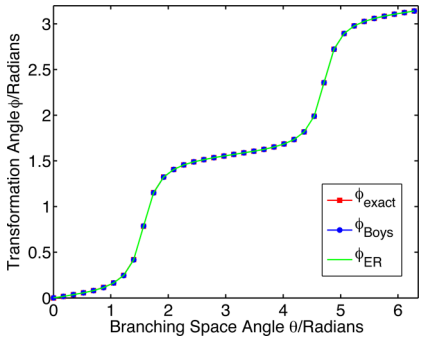

Figure 9. Mixing angle ϕ between adiabatic and diabatic states versus branching space angle θ at r = 0.001 Å. These data show that localized diabatization can recover the topology of at least one CI almost exactly.

A few words are now in order regarding the stunning agreement in Figure 9. Even if localized diabatization were to generate exactly diabatic electronic states with zero diabatic coupling and the correct **g**−**h** plane, the agreement in Figure 9 need not be expected. After all, when we calculated **g** and **h** by analyzing the energy difference between adiabatic surfaces in the **g**−**h** plane, the **g** and **h** vectors were not unique (even though they were required to be perpendicular). Thus, one could switch **g** for **h** and vice versa. Moreover, **g** and **h** do not even need to be perpendicular for a general diabatic basis. The agreement in Figure 9 demonstrates, however, that by maximizing charge localization, Boys and ER localized diabatization seek diabatic states with maximal energy separation, and this feature agrees with our earlier definition of **g**. Lastly, note that in Figure 9 when θ is increased from 0 to 2π, the mixing angle is changed by a factor of π, i.e., $|\Xi(\theta)\rangle = -|\Xi(\theta + 2\pi)\rangle$. This is the expected Berry's phase behavior for a loop around a CI.[39,76]

Before finishing this subsection, we observe that if the radius of the loop around the CI is increased, the agreement between ϕ_{Boys}/ϕ_{ER} and ϕ_{exact} is preserved over a relatively long range, as shown in Figure 10. When the radius is as large as 0.3 Å, ϕ_{exact} still agrees roughly with the localized diabatization results even though the potential energies have changed dramatically. This demonstrates that the first-order Hamiltonian is a good approximation when we look locally at the CI in the **g**−**h** plane.

V. PHOSPHORESCENCE LIFETIME OF BENZALDEHYDE

The final relaxation step of benzaldehyde is phosphorescence to the ground state. Extensive experimental results show that T_1 is the electronic state that accounts for benzaldehyde's phosphorescence character.[5,6,17,21,22] Theory predicts that the T_1 state strongly couples with the ground state according to the El-Sayed rules, and this is also confirmed by our spin−orbit coupling constant calculation. For each spin polarization, the phosphorescence lifetime of benzaldehyde from the T_1 state was calculated by[77]

$$\frac{1}{\tau_k} = \frac{4}{3\hbar c^3}(\Delta E^k)^3 \sum_\alpha \left\| M_\alpha^k \right\|^2 \quad (35)$$

where $k = 0, \pm 1$ refers to different polarizations of the T_1 state, ΔE^k is the transition energy, and $M_\alpha{}^k$ is the electric transition

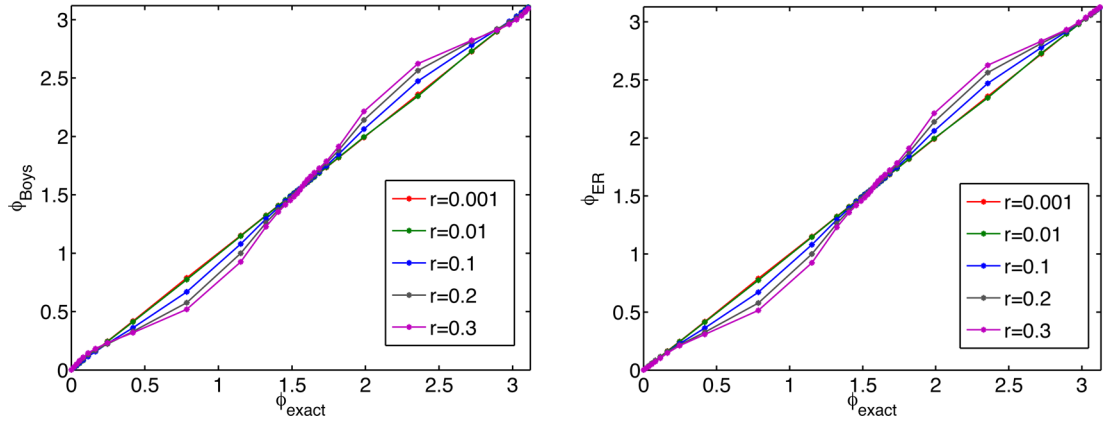

Figure 10. Exact mixing angle versus localized diabatization results. r refers to the distances (in Å) of the circular loop surrounding the CI point in the **g**−**h** plane. For each loop, 36 single-point calculations were performed.

dx.doi.org/10.1021/jp405574q | J. Phys. Chem. C 2013, 117, 19839−19849

dipole moment between the ground state and the triplet state. $\alpha = x, y, z$ refers to different components of the dipole moment. The final expression of M_α^k is

$$M_\alpha^k = \sum_{n=0}^{\infty} \frac{\langle S_0|\mu_\alpha|S_n\rangle\langle S_n|H_{SO}|T_1^k\rangle}{E(S_n) - E(T_1)} + \sum_{n=1}^{\infty} \frac{\langle S_0|H_{SO}|T_n\rangle\langle T_n|\mu_\alpha|T_1^k\rangle}{E(T_n) - E(S_0)} \quad (36)$$

The averaged phosphorescence lifetime is given by

$$\frac{1}{\tau} = \frac{1}{3}\sum_{k=0,\pm1}\frac{1}{\tau_k} \quad (37)$$

Because only a finite number of excited states in eq 36 can be included in our calculations, we tested up to 25 singlet states and 25 (triply degenerate) triplet states in this work (Figure 11). All calculations were carried out at the T_1 state optimized geometry. The averaged phosphorescence lifetime converges at 1.81×10^{-3} s, which is comparable to the experimental data (7.12×10^{-4} s) given by Biron and Longin for gas phase benzaldehyde at zero pressure.[21]

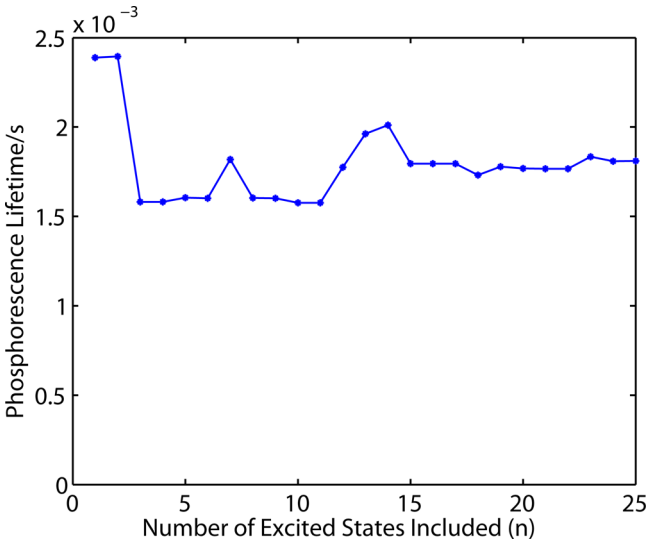

Figure 11. Averaged phosphorescence lifetime ($1/\tau$ in eq 37) including variable numbers of excited states (n in eq 36).

VI. CONCLUSION AND OUTLOOK

We have analyzed the cascade of relaxation steps experienced by photoexcited benzaldehyde. Using TD-DFT/ωB97X, we have roughly recovered previous experimental and CASSCF/CASPT2 results for all optimized geometries and excitation energies. Spin−orbit coupling calculations were carried out, and we found a strong spin−orbit coupling between the S_1 and T_2 states, leading to a very fast ISC process ($k_{ISC} = 8.03 \times 10^{10}$ s^{-1}). The IC between T_2 and T_1 was shown to be mediated via a CI and we have verified our capacity to generate meaningful diabatic states using the techniques of localized diabatization. Finally, we have calculated a phosphorescence lifetime of 1.81×10^{-3} s for the $T_1 \rightarrow S_0$ transition.

To address the IC between T_2 and T_1, Izmaylov et al.[78] have formulated recently a nonequilibrium generalization of the Fermi golden rule which can deal with the dynamics of electronic transitions through a CI in the limiting case of a linear Hamiltonian. Unfortunately, thus far we have been unable to globally fit our potential energy surfaces and couplings to a first-order Hamiltonian. Going forward, given our interest in recovering the proper T_2/T_1 dynamics, we will need to either (i) redouble our efforts and explore all of parameter space for a reasonable fit to a linear Hamiltonian and then apply ref 78 or (ii) include higher-order terms so as to fit the data more closely and then develop a new dynamical model. This work is ongoing.

AUTHOR INFORMATION

Corresponding Author

*E-mail: subotnik@sas.upenn.edu. Phone: 215-746-7078

Notes

The authors declare no competing financial interest.

ACKNOWLEDGMENTS

We thank Ethan Alguire, Spiridoula Matsika, Joe Ivanic, and Yihan Shao for their helpful conversations and computational guidance. This work was supported by National Science Foundation CAREER Grant CHE-1150851; J.E.S. also acknowledges an Alfred P. Sloan Research Fellowship and a David and Lucille Packard Fellowship.

REFERENCES

(1) Ohmori, N.; Suzuki, T.; Ito, M. Why Does Intersystem Crossing Occur in Isolated Molecules of Benzaldehyde, Acetophenone, and Benzophenone? *J. Phys. Chem.* **1988**, *92* (5), 1086−1093.
(2) Berger, M.; Goldblatt, I. L.; Steele, C. Photochemistry of Benzaldehyde. *J. Am. Chem. Soc.* **1973**, *95* (6), 1717−1725.
(3) Silva, C. R.; Reilly, J. P. Theoretical Calculations on Excited Electronic States of Benzaldehyde and Observation of the $S_2 \leftarrow S_0$ Jet-Cooled Spectrum. *J. Phys. Chem.* **1996**, *100* (43), 17111−17123.
(4) Smolarek, J.; Zwarich, R.; Goodman, L. Active Out-of-plane Modes in $1A''(n-\pi^*) \leftarrow S_0$ of Benzaldehyde Vapor. *J. Mol. Spectrosc.* **1972**, *43* (3), 416−428.
(5) Hirata, Y.; Lim, E. C. Nonradiative Electronic Relaxation of Gas Phase Aromatic Carbonyl Compounds: Benzaldehyde. *J. Comput. Chem.* **1980**, *72* (10), 5505−5510.
(6) Bagchi, A.; Huang, Y.; Xu, Z.; Raghunath, P.; Lee, Y.; Ni, C.; Lin, M.; Lee, Y. Photodissociation Dynamics of Benzaldehyde (C_6H_5CHO) at 266, 248, and 193 nm. *Chem.—Asian. J.* **2011**, *6* (11), 2961−2976.
(7) Metcalfe, J.; Brown, R. G.; Phillips, D. Photophysical Processes in Benzaldehyde. *J. Chem. Soc. Faraday Trans. 2* **1975**, *71*, 409−413.
(8) Molina, V.; Merchan, M. Theoretical Analysis of the Electronic Spectra of Benzaldehyde. *J. Phys. Chem. A* **2001**, *105* (15), 3745−3751.
(9) Cui, G.; Lu, Y.; Thiel, W. Electronic Excitation Energies, Three-State Intersections, and Photodissociation Mechanisms of Benzaldehyde and Acetophenone. *Chem. Phys. Lett.* **2012**, *537*, 21−26.
(10) Fang, W. Ab Initio Determination of Dark Structures in Radiationless Transitions for Aromatic Carbonyl Compounds. *Acc. Chem. Res.* **2008**, *41* (3), 452−457.
(11) Turro, N. J.; Ramamurthy, V.; Scaiano, J. *Principles of Molecular Photochemistry: An Introduction*; University Science Books: South Orange, NJ, 2009.
(12) Bruhlmann, U.; Nonella, M.; Russegger, P.; Huber, J. R. The Triplet State Decay $(T_1(n\pi^*) \rightarrow S_0)$ of Benzaldehydes in the Dilute Gas Phase. *Chem. Phys.* **1983**, *81* (3), 8439−8447.
(13) Long, S. R.; Meek, J. T.; Harrington, P. J.; Reilly, J. P. Benzaldehyde Photochemistry Studied with Laser Ionization Mass and Photoelectron Spectroscopy. *J. Chem. Phys.* **1983**, *78* (6), 3341−3343.
(14) Yang, J. J.; Gobeli, D. A.; El-Sayed, M. A. Wavelength Dependence of the Multiphonon Ionization-Fragmentation Mass

Spectrometric Pattern of Benzaldehyde. *J. Phys. Chem.* **1983**, *87*, 2255−2260.
(15) Yang, J. J.; Gobeli, D. A.; El-Sayed, M. A. Change in the Mechanism of Laser Multiphoton Ionization−Dissociation in Benzaldehyde by Changing the Laser Pulse Width. *J. Phys. Chem.* **1985**, *89*, 3426−3429.
(16) Feenstra, J. S.; Park, S. T.; Zewail, A. H. Excited State Molecular Structures and Reactions Directly Determined by Ultrafast Electron Diffraction. *J. Chem. Phys.* **2005**, *123*, 221104.
(17) Park, S. T.; Feenstra, J. S.; Zewail, A. H. Ultrafast Electron Diffraction: Excited State Structures and Chemistries of Aromatic Carbonyls. *J. Chem. Phys.* **2006**, *124* (17), 174707.
(18) Lee, S.; Tang, K.; Chen, I.; Schmitt, M.; Shaffer, J. P.; Schultz, T.; Underwood, J. G.; Zgierski, M. Z.; Stolow, A. Substituent Effects in Molecular Electronic Relaxation Dynamics via Time-Resolved Photoelectron Spectroscopy: $\pi\pi^*$ States in Benzenes. *J. Phys. Chem. A* **2002**, *106* (39), 8979−8991.
(19) Liu, B.; Wang, B.; Wang, Y.; Wang, L. Wavelength-Dependent Photodissociation Dynamics of Benzaldehyde. *Chin. J. Chem. Phys.* **2009**, *22* (6), 587−591.
(20) Itoh, T. The Evidence Showing that the Intersystem Crossing Yield of Benzaldehyde Vapour Is Unity. *Chem. Phys. Lett.* **1988**, *151* (1−2), 166−168.
(21) Biron, M.; Longin, P. Triplet Dynamics of Gas-Phase Benzaldehyde after Excitation of the Forbidden $T_1(n, \pi^*) \leftarrow S_0$ Transition. *Chem. Phys. Lett.* **1985**, *116* (2−3), 250−253.
(22) Sneh, O.; Cheshnovsky, O. Dynamics of Triplet States in Beam-Isolated Benzaldehyde. *J. Phys. Chem.* **1991**, *95* (19), 7154−7164.
(23) Ridley, J. E.; Zerner, M. C. Calculated Spectra of Benzaldehyde and Benzoic Acid. *J. Mol. Spectrosc.* **1979**, *76* (1−3), 71−85.
(24) Fang, W.; Phillips, D. L. The Crucial Role of the $S_1/T_2/T_1$ Intersection in the Relaxation Dynamics of Aromatic Carbonyl Compounds upon $n \rightarrow \pi^*$ Excitation. *Chem. Phys. Chem.* **2002**, *3* (10), 889−892.
(25) Wang, Y.; He, H.; Fang, W. An Accurate Prediction of Adiabatic Excitation Energies to the Low-Lying Electronic States for Acetophenone and the Related Carbonyl Compounds. *J. Mol. Spectrosc.* **2003**, *634*, 281−287.
(26) Olmsted, J., III; El-Sayed, M. Phosphorescence Spectrum and Mechanisms of Benzaldehyde in Methyl-Cyclohexane at 4.2 K. *J. Mol. Spectrosc.* **1971**, *40* (1), 71−83.
(27) Kiritani, M.; Yoshii, T.; Hirota, N.; Baba, M. Intramolecular Radiationless Transitions in Substituted Benzaldehydes. *J. Phys. Chem.* **1994**, *98*, 11265−11268.
(28) El-Sayed, M. A. The Triplet State: Its Radiative and Nonradiative Properties. *Acc. Chem. Res.* **1968**, *1* (1), 8−16.
(29) Chai, J.; Head-Gordon, M. Systematic Optimization of Long-Range Corrected Hybrid Density Functionals. *J. Chem. Phys.* **2009**, *131* (17), 174105.
(30) Kong, J.; Lee, M. S.; Lee, A. M.; Gwaltney, S. R.; Adams, T. R.; Ochsenfeld, C.; Gilbert, A. T. B.; Kedziora, G. S.; Rassolov, V. A.; Maurice, D. R.; Nair, N.; Shao, Y.; Besley, N. A.; Maslen, P. E.; Dombroski, J. P.; Daschel, H.; Zhang, W.; Korambath, P. P.; Baker, J.; Byrd, E. F. C.; Voorhis, T. V.; Oumi, M.; Hirata, S.; Hsu, C.-P.; Ishikawa, N.; Florian, J.; Warshel, A.; Johnson, B. G.; Gill, P. M. W.; Head-Gordon, M.; Pople, J. A. Q-Chem 2.0: A High-Performance Ab Initio Electronic Structure Program Package. *J. Comput. Chem.* **2000**, *21*, 1532−1548.
(31) Head-Gordon, M.; Grana, A. M.; Maurice, D.; White, C. A. Analysis of Electronic Transitions as the Difference of Electron Attachment and Detachment Densities. *J. Phys. Chem.* **1995**, *99*, 14261−14270.
(32) Subotnik, J. E. Configuration Interaction Singles Has a Large Systematic Bias against Charge-Transfer States. *J. Chem. Phys.* **2011**, *135*, 071104.
(33) Abegg, P. W. Ab Initio Calculation of Spin−Orbit Coupling Constants for Gaussian Lobe and Gaussian-type Wave Functions. *Mol. Phys.* **1975**, *30* (2), 579−596.
(34) Recall that T_2 denotes the $\pi-\pi^*$ diabatic triplet state. In these calculations, the excitation amplitudes t_i^a for T_2 were obtained from the Boys localized diabatization method in Q-Chem discussed in Section IV.D.
(35) Marcus, R. A. On the Theory of Oxidation-Reduction Reactions Involving Electron Transfer. V. Comparison and Properties of Electrochemical and Chemical Rate Constants. *J. Phys. Chem.* **1963**, *67*, 853−857.
(36) Nitzan, A. *Chemical Dynamics in Condensed Phases*; Oxford University Press: Oxford, U.K., 2006.
(37) Subotnik, J. E.; Vura-Weis, J.; Sodt, A. J.; Ratner, M. A. Predicting Accurate Electronic Excitation Transfer Rates via Marcus Theory with Boys or Edmiston−Ruedenberg Localized Diabatization. *J. Phys. Chem. A* **2010**, *114* (33), 8665−8675.
(38) Jablonski Diagram. http://chemwiki.ucdavis.edu/Physical_Chemistry/Spectroscopy/Electronic_Spectroscopy/Jablonski_diagram.
(39) Domcke, W.; Yarkony, D. R.; Koppel, H. *Conical Intersections: Electron Structure Dynamics and Spectroscopy*; World Scientific Publishing Co. Pte. Ltd.: Singapore, 2004.
(40) Martinez, T. J.; Ben-Nun, M.; Levine, R. D. Multi-Electronic-State Molecular Dynamics: A Wave Function Approach with Applications. *J. Phys. Chem.* **1996**, *100*, 7884−7895.
(41) Ben-Nun, M.; Martinez, T. J. A Multiple Spawning Approach to Tunneling Dynamics. *J. Chem. Phys.* **2000**, *112*, 6113−6121.
(42) Matsika, S.; Krause, P. Nonadiabatic Events and Conical Intersections. *Annu. Rev. Phys. Chem.* **2011**, *62*, 621−643.
(43) Bernardi, F.; Olivucci, M.; Robb, M. A. Predicting Forbidden and Allowed Cycloaddition Reactions: Potential Surface Topology and Its Rationalization. *Acc. Chem. Res.* **1990**, *23*, 405−412.
(44) Yarkony, D. R. Current Issues in Nonadiabatic Chemistry. *J. Phys. Chem.* **1996**, *100* (48), 18612−18628.
(45) Yarkony, D. R. Conical Intersections: The New Conventional Wisdom. *J. Phys. Chem. A* **2001**, *105* (26), 6277−6293.
(46) Jasper, A. W.; Zhu, C.; Nangia, S.; Truhlar, D. G. Introductory Lecture: Nonadiabatic Effects in Chemical Dynamics. *Farad. Discuss.* **2004**, *127*, 1−22.
(47) Matsika, S. Conical Intersections in Molecular Systems. *Rev. Comput. Chem.* **2007**, *23*, 83−124.
(48) Yarkony, D. R. Systematic Determination of Intersections of Potential Energy Surfaces Using a Lagrange Multiplier Constrained Procedure. *J. Phys. Chem.* **1993**, *97*, 4407−4412.
(49) Benjamin, L. G.; Joshua, C. D.; Todd, M. J. Optimizing Conical Intersections without Derivative Coupling Vectors: Application to Multistate Multireference Second-Order Perturbation Theory (MS-CASPT2). *J. Phys. Chem. B* **2008**, *112* (2), 405−413.
(50) Baer, M. Adiabatic and Diabatic Representations for Atom−Molecule Collisions: Treatment of the Collinear Arrangement. *Chem. Phys. Lett.* **1975**, *35*, 112−118.
(51) Mead, C. A.; Truhlar, D. G. Conditions for the Definition of a Strictly Diabatic Electronic Basis for Molecular Systems. *J. Chem. Phys.* **1982**, *77*, 6090−6098.
(52) Sadygov, R. G.; Yarkony, D. R. On the Adiabatic to Diabatic States Transformation in the Presence of a Conical Intersection: A Most Diabatic Basis from the Solution to a Poissons Equation. I. *J. Chem. Phys.* **1998**, *109*, 20−25.
(53) Ruedenberg, K.; Atchity, G. J. A Quantum Chemical Determination of Diabatic States. *J. Chem. Phys.* **1993**, *99*, 3799−3803.
(54) Atchity, G. J.; Ruedenberg, K. Determination of Diabatic States through Enforcement of Configurational Uniformity. *Theor. Chem. Acc.* **1997**, *97*, 47−58.
(55) Nakamura, H.; Truhlar, D. G. The Direct Calculation of Diabatic States Based on Configurational Uniformity. *J. Chem. Phys.* **2001**, *115*, 10353−10372.
(56) Nakamura, H.; Truhlar, D. G. Direct Diabatization of Electronic States by the Fourfold Way, II: Dynamical Correlation and Rearrangement Processes. *J. Chem. Phys.* **2002**, *117*, 5576−5593.
(57) Nakamura, H.; Truhlar, D. G. Extension of the Fourfold way for Calculation of Global Diabatic Potential Energy Surfaces of Complex,

Multiarrangement, Non-Born−Oppenheimer Systems: Application to HNCO(S_0,S_1). *J. Chem. Phys.* **2003**, *118*, 6816−6829.
(58) Pacher, T.; Cederbaum, L. S.; Koppel, H. Approximately Diabatic States from Block Diagonalization of the Electronic Hamiltonian. *J. Chem. Phys.* **1988**, *89*, 7367−7381.
(59) Pacher, T.; Cederbaum, L. S.; Koppel, H. Adiabatic and Quasidiabatic States in a Gauge Theoretical Framework. *Adv. Chem. Phys.* **1993**, *84*, 293−391.
(60) Cave, R. J.; Newton, M. D. Generalization of the Mulliken−Hush Treatment for the Calculation of Electron Transfer Matrix Elements. *Chem. Phys. Lett.* **1996**, *249*, 15−19.
(61) Cave, R. J.; Newton, M. D. Calculation of Electronic Coupling Matrix Elements for Ground and Excited State Electron Transfer Reactions: Comparison of the Generalized Mulliken−Hush and Block Diagonalization Methods. *J. Chem. Phys.* **1997**, *106*, 9213−9216.
(62) Werner, H. J.; Meyer, W. MCSCF study of the avoided curve crossing of the two lowest $1\Sigma^+$ states of LiF. *J. Chem. Phys.* **1981**, *74*, 5802−5807.
(63) Subotnik, J. E.; Yeganeh, S.; Cave, R. J.; Ratner, M. A. Constructing Diabatic States from Adiabatic States: Extending Generalized Mulliken−Hush to Multiple Charge Centers with Boys Localization. *J. Chem. Phys.* **2008**, *129* (24), 244101.
(64) Subotnik, J. E.; Cave, R. J.; Steele, R. P.; Shenvi, N. The Initial and Final States of Electron and Energy Transfer Processes: Diabatization as Motivated by System-Solvent Interactions. *J. Chem. Phys.* **2009**, *130*, 234102.
(65) Voityuk, A. A.; Rosch, N. Fragment Charge Difference Method for Estimating Donor-Acceptor Electronic Coupling: Application to DNA π-stacks. *J. Chem. Phys.* **2002**, *117*, 5607−5616.
(66) Hsu, C. P.; You, Z. Q.; Chen, H. C. Characterization of the Short-Range Couplings in Excitation Energy Transfer. *J. Phys. Chem. C* **2008**, *112*, 1204−1212.
(67) Chen, H. C.; You, Z. Q.; Hsu, C. P. The Mediated Excitation Energy Transfer: Effects of Bridge Polarizability. *J. Chem. Phys.* **2008**, *129*, 084708.
(68) Hsu, C. P. The Electronic Couplings in Electron Transfer and Excitation Energy Transfer. *Acc. Chem. Res.* **2009**, *42*, 509−518.
(69) Wu, Q.; Voorhis, T. V. Direct Optimization Method to Study Constrained Systems within Density-Functional Theory. *Phys. Rev. A* **2005**, *72*, 024502.
(70) Wu, Q.; Voorhis, T. V. Constrained Density Functional Theory and Its Application in Long-Range Electron Transfer. *J. Chem. Theory Comp.* **2006**, *2*, 765−774.
(71) Wu, Q.; Voorhis, T. V. Direct Calculation of Electron Transfer Parameters through Constrained Density Functional Theory. *J. Phys. Chem. A* **2006**, *110*, 9212−9218.
(72) Wu, Q.; Voorhis, T. V. Extracting Electron Transfer Coupling Elements from Constrained Density Functional Theory. *J. Chem. Phys.* **2006**, *125*, 164105.
(73) Foster, J. M.; Boys, S. F. Canonical Configurational Interaction Procedure. *Rev. Mod. Phys.* **1960**, *32*, 300−302.
(74) Edmiston, C.; Ruedenberg, K. Localized Atomic and Molecular Orbitals. *Rev. Mod. Phys.* **1963**, *35*, 457−465.
(75) Note that Koppel and co-workers have recently suggested a very clever nonlocal diabatization scheme near a CI.[79,80]
(76) Berry, M. V. *Proc. R. Soc. London, Ser. A* **1984**, *392*, 45−57.
(77) Jansson, E.; Norman, P.; Minaev, B.; Agren, H. Evaluation of Low-Scaling Methods for Calculation of Phosphorescence Parameters. *J. Chem. Phys.* **2006**, *124* (11), 114106.
(78) Izmaylov, A. F.; Mendive-Tapia, D.; Bearpark, M. J.; Robb, M. A.; Tully, J. C.; Frisch, M. J. Nonequilibrium Fermi Golden Rule for Electronic Transitions through Conical Intersections. *J. Chem. Phys.* **2011**, *135*, 234106.
(79) Thiel, A.; Koppel, H. Quantal Phase Factors Accompanying Adiabatic Changes. *J. Chem. Phys.* **1999**, *100*, 9371−9383.
(80) Koppel, H.; Gronki, J.; Mahapatra, S. Construction Scheme for Regularized Diabatic States. *J. Chem. Phys.* **2001**, *115*, 2377−2388.